Heliyon 5 (2019) e02738

Contents lists available at ScienceDirect

Heliyon

journal homepage: www.heliyon.com

Research article

# Synthesis, X-ray crystal structure, Hirshfeld surface analysis, and molecular docking study of novel inhibitor of hepatitis B: methyl 4-fluoro-3-(morpholinosulfonyl)benzo[b]thiophene-2-carboxylate

Alexandre V. Ivachtchenko [a], Oleg D. Mitkin [a,*], Dmitry V. Kravchenko [b], Sergiy M. Kovalenko [a,c,f], Svitlana V. Shishkina [c,e,f], Natalya D. Bunyatyan [c,d], Irina S. Konovalova [e], Irina G. Dmitrieva [b], Vladimir V. Ivanov [f], Thierry Langer [g]

[a] ChemRar Research and Development Institute, 7 Nobel st., Innovation Center Skolkovo Territory, Moscow, 143026, Russia
[b] Chemical Diversity Research Institute, 2A Rabochaya st., Khimki, Moscow Region, 141400, Russia
[c] Federal State Autonomous Educational Institution of Higher Education I.M. Sechenov First Moscow State Medical University of the Ministry of Healthcare of the Russian Federation (Sechenovskiy University), 8 Trubeckaya st., Moscow, 119991, Russia
[d] Federal State Budgetary Institution "Scientific Centre for Expert Evaluation of Medicinal Products" of the Ministry of Health of the Russian Federation, Petrovsky Boulevard 8, bld. 2, Moscow, 127051, Russia
[e] State Scientific Institution "Institute for Single Crystals" of the National Academy of Sciences of Ukraine, 61001, Kharkov, Ukraine
[f] V.N.Karazin Kharkiv National University, 4 Svobody sq., Kharkiv, 61077, Ukraine
[g] Department of Pharmaceutical Chemistry, University of Vienna, Althanstraße 14, A-1090, Vienna, Austria

ARTICLE INFO

*Keywords:*
Organic chemistry
Theoretical chemistry
Pharmaceutical chemistry
Hepatitis B
HBV
Pharmaceutical crystals
4-Fluoro-3-(morpholinosulfonyl)benzo[b]thiophene-2-carboxylate
Benzothiophene
Hydrogen bond
Hirshfeld surface analysis
Molecular docking study

ABSTRACT

A method of 4-fluoro-3-(morpholinosulfonyl)benzo[b]thiophene-2-carboxylate synthesis has been developed and the electronic and spatial structure of a new biologically active molecule has been studied both theoretically and experimentally. The title compound was crystallized from acetonitrile and the single crystal X-ray analysis has revealed that it exists in a monoclinic $P2_1/c$ space group, with one molecule in the asymmetric part of the unit cell. Hirshfeld surface analysis was used to study intermolecular interactions in the crystal. Molecular docking study evaluates the investigated compound as a new potential inhibitor of hepatitis B. Testing for anti-hepatitis B virus activity has shown that this substance demonstrates *in vitro* nanomolar inhibitory activity against HBV.

## 1. Introduction

Benzothiophene and its derivatives belong to an important class of heterocyclic compounds that have been extensively exploited in medical chemistry, natural products, and materials science [1, 2, 3, 4]. Among them, 3-substituted benzothiophenes are especially important since many pharmaceuticals as well as drug candidates contain this scaffold [5, 6, 7] (Fig. 1).

Despite the wide spectrum of biological activity of this scaffold, this range can be supplemented by introducing of certain functional groups, in particular, a fluorine atom, which is often used to modify drugs (about 25% of new drugs contain at least one fluorine atom or trifluoromethyl group). A fluorine atom can significantly affect the binding of a biologically active substance to receptors, the flow of metabolism and membrane permeability [8]. Of particular interest is the introduction of a sulfamide group into the molecule, which can lead to the appearance of antibacterial, diuretic, hypoglycemic, antiseptic and other types of pharmacological activity [9]. However, to date, only a few patents are known in which sulfamide derivatives of benzo[b] thiophene were reported and their use for inhibiting the binding of an endothelin peptide to an endothelin receptor is proposed [10, 11, 12, 13]. Morpholine moiety is also often employed in the field of medicinal chemistry for its

* Corresponding author.
*E-mail address:* mod.chemdiv@gmail.com (O.D. Mitkin).

https://doi.org/10.1016/j.heliyon.2019.e02738
Received 10 September 2019; Received in revised form 2 October 2019; Accepted 23 October 2019

advantageous physicochemical, biological, and metabolic properties. A large body of in vivo studies has demonstrated morpholine's potential to improve pharmacokinetics in addition to promising drag-likeness [14]. Therefore, it is of substantial interest to develop efficient methods for the synthesis of such structures and their derivatives and to study their pharmacological potential. In this paper, we turned our attention to study anti-hepatitis B virus activity of the mentioned structures relatively to their electronic and spatial structure. The mentioned 3-substituted benzothiophenic core was synthesized and the title molecule was chosen in frames of wide row potentially pharmacophoric small molecules testing

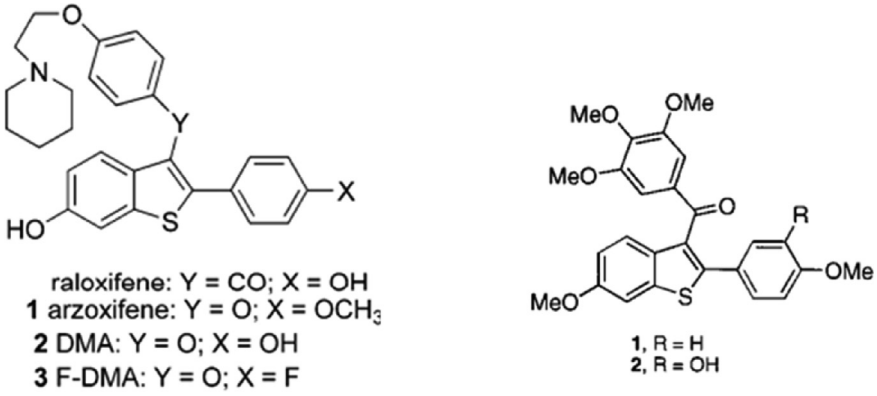


**Fig. 1.** Structure of 3-substituted benzothiophenes which are used as drugs and drug candidates.

in newly designed HBV-infection model with the usage of human hepatoma line HepG [15] as an optimal result of activity – cytotoxicity analysis. The model was elaborated in our laboratories and described earlier in [16].

Despite significant progress in the etiology of viral hepatitis studying, the incidence of this disease remains quite high especially due to resistance from time to time evolving on the therapeutic course. Hepatitis B is an infectious inflammatory liver disease that occurs as a result of the introduction of HBV into the body and is a serious global public health problem. It can cause both acute and chronic diseases and put people at high risk of death from cirrhosis and liver cancer. Despite the presence of an effective HBV prophylactic vaccine, the burden of chronic HBV infection is still a serious unmet global medical problem due to suboptimal treatment options and a steady new infection rate in most parts of the developing world. In this regard an acute demand for novel HBV therapeutic agents that improve treatment or/and prevent HBV infection still exists. Therefore, the search for new drugs for the treatment of hepatitis B is an actual and important task. In a continuation of our efforts to obtain a new HBV inhibitor for treatment and prevention of human HBV infections [16, 17, 18], we initiated design, synthesis, and anti-hepatitis B virus activity testing of a new methyl 4-fluoro-3-(morpholinosulfonyl)benzo[b]thiophene-2-carboxylate (Fig. 2).

Single crystal X-ray analysis and different spectroscopic techniques assured the assigned chemical structure of the title compound. In addition, Hirshfeld surface analysis, conformational analysis and molecular docking simulations were also executed for the title compound.

## 2. Experimental

### 2.1. Materials and methods

All chemicals were obtained from Sigma-Aldrich or Merck. NMR Spectra were registered on Bruker DPX 300 spectrometer at room temperature (298K) on a using DMSO-d6 as the solvent and processed using Bruker XWinNMR software. LC/MS was developed by means of chromatography with PHENOMENEX GEMINI NX C18 110Å 4.61 × 150 mm column (0.05% TFA, gradient MeCN/$H_2O$), UV-detector SHIMADZU SPD-10AD VP (registered absorption at 254 nm), ELSD (evaporative light scattering detector) SEDEX-75 and API-150EX mass-spectrometer. Elution started with 0.1 M solution of TFA in water and ended with 0.1 M solution of TFA in acetonitrile used a linear gradient at a flow rate of 0.15 mL/min and an analysis cycle time of 25 min. FT-IR spectrum was registered in KBr pellet with Shimadzu IR Prestige-21 Fourier Transform Infrared (FTIR) Spectrophotometer. UV/Vis spectrum was registered in acetonitrile with Agilent 8453 UV-Vis Spectrophotometer. Melting point was registered with Buchi M-560. Elemental analysis was performed on EuroEA-3000 CHNS-O Analyzer.

#### 2.1.1. Methyl 3-(chlorosulfonyl)-4-fluorobenzo[b]thiophene-2-carboxylate (2)

3-Amino-4-fluorobenzo[b]thiophene-2- carboxylate (1) (126 g, 0.6 mol) was added in one portion to a mixture of concentrated hydrochloric acid (200 mL) and glacial acetic acid (100 mL) in a 1000-mL beaker arranged for efficient mechanical stirring. The white hydrochloride salt was precipitated. The beaker was placed in a dry ice-ethanol bath and, when the temperature of the stirred mixture reached -10 °C, a solution of sodium nitrite (44.9 g, 0.65 mol) in water (65 mL) was added drop wise so fast that the temperature did not exceed -5 °C. After the sodium nitrite solution has been completely added, the mixture was stirred for 45 min while the temperature was retained between -10 °C and -5 °C. While the diazotization was being completed, glacial acetic acid (600 mL) was placed in a 4000-mL beaker and cuprous chloride (15 g, 0.15 mol) was added with magnetic stirring. Sulfur dioxide was bubbled through a bubbler tube with a fritted end immersed below the surface of the acetic acid until saturation was completed and the yellow-green suspension became blue-green. Most of the solids dissolved during this time (20–30 min). Then the mixture was placed in an ice bath and cooled with stirring. When the temperature approached 10 °C, the diazotization solution was added portion wise over a 30 min period to the sulfur dioxide reaction mixture. Considerable foaming occurred after each addition, and a few drops of ether could be added to break it. The temperature increased during the addition, but it should not exceed 30 °C. After the diazonium salt mixture had been added, the whole reaction mixture was poured into ice-water mixture (1 : 1, 2000 mL), stirred magnetically until the ice had melted, and transferred to a 4000-mL separatory funnel. The product was separated as a dark-yellow oil. The aqueous layer was extracted with 200-mL portions of $CHCl_3$, and these extracts were added to the initial product. The combined organic layer was washed with saturated aqueous sodium bicarbonate until neutral, then with water, and then dried over magnesium sulphate and concentrated. Yield 111 g (60%), dark yellow viscous liquid. The product (2) was used for the next reaction stage without additional purification.

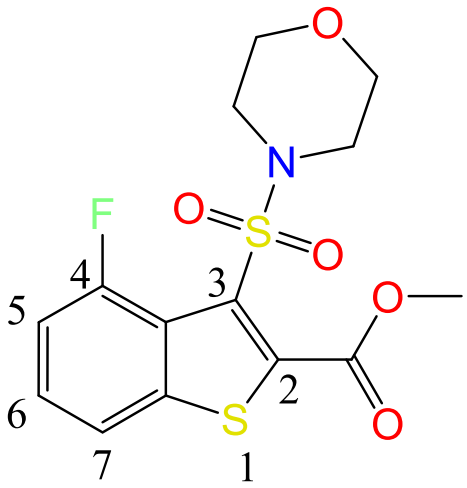


**Fig. 2.** Chemical structure of the title compound (4).

*2.1.2. Methyl 4-fluoro-3-(morpholinosulfonyl)benzo[b]thiophene-2-carboxylate (4)*

A solution of compound (2) (1.0 mmol, 309 mg) and 1.1 mmol of morpholine (3) in DMF (5 mL) was stirred for 1 h at 60 °C. After cooling, water (20 mL) was added and the formed solid was filtered off and recrystallized from aqueous i-PrOH (10 mL).

Yield 259 mg (72%), white crystal-like powder, m.p. 93.2–95.0 °C; UV (Acetonitrile) $\lambda_{max}$ (nm) 204, 234, 262, 271, 298, 303 (Figure S1); IR (KBr): $\nu$ (cm–1) 3069, 3011, 2964, 2908, 2872 (C–H), 1729 (C=O), 1608, 1561, 1497, 1465, 1452, 1358, 1266, 1247, 1167, 1112, 1077,963, 947, 929, 853, 793, 769, 737, 674, 591, 512 (Figure S2); 1H NMR (300 MHz, DMSO-d6) δ 3.26 (t, 4H, J = 4.3 Hz, $_{NCH2}$), 3.59 (t, 4H, J = 4.3 Hz, OCH2), 3.92 (s, 3H, $OCH_3$), 7.44 (ddd, 1H, J = 1,0, 8.1, 12.3 Hz, H-5), 7.65 (td, 1H, J = 4.6, 8.1 Hz, H-6), 8.06 (dd, 1H, J = 1.0, 8.1 Hz, H-7) (Figure S5); 13C NMR (75 MHz, DMSO-d6) δ 45.16 (2C, $NCH_2$), 54.00 ($OCH_3$), 65.89 (2C, $OCH_2$), 113.21 (d, J = 21.3 Hz), 120.12 (d, J = 4.2 Hz), 121.42 (d, J = 16.9 Hz), 127.60 (d, J = 4.7 Hz), 128.65 (d, J = 8.0 Hz), 140.32 (d, J = 5.2 Hz), 142.81, 156.25 (d, J = 255.5 Hz, C-4), 162.55 (Figure S4); 19F NMR (377 MHz, DMSO-d6) δ -107.59 (dd, J = 4.5, 12.2 Hz) (Figure S3); LC/MS m/z (%): 360.4 [MH]+ (99) (Figure S6); Found, %: C 46.92; H 3.83; N 3.99. $C_{14}H_{14}FNO_5S_2$. Calculated, %: 46.79; H 3.90; N 3.93.

Further crystallization by slow evaporation of *i*-propanol solution was carried out to provide single block colourless crystals suitable for X-ray diffraction analysis (Fig. 3).

### 2.2. X-ray experimental part

The crystals of compound (4) ($C_{14}H_{14}FNO_5S_2$) are monoclinic. At 293 K $a = 10.1712(7)$, $b = 19.8982(1)$, $c = 7.6814(6)$ Å, $\beta = 95.347(7)°$, V = 1547.9(2) $Å^3$, $M_r = 359.40$, Z = 4, space group $P2_1/c$, $d_{calc} = 1.542$ g/$cm^3$, m(MoKa) = 0.379 $mm^{-1}$, F(000) = 744. Intensities of 11494 reflections (2719 independent, $R_{int} = 0.088$) were measured on the «Xcalibur-3» diffractometer (graphite monochromated $MoK_\alpha$ radiation, CCD detector, ω-scaning, $2\Theta_{max} = 50°$).

The structure was solved by direct method using SHELXTL package [19]. Position of the hydrogen atoms were located from electron density difference maps and refined by "riding" model with $U_{iso} = nU_{eq}$ of the carrier atom (n = 1.5 for methyl group and n = 1.2 for other hydrogen atoms). Full-matrix least-squares refinement of the structures against $F^2$ in anisotropic approximation for non-hydrogen atoms using 2719 reflections was converged to: $wR_2 = 0.164$ ($R_1 = 0.065$ for 1788 reflections with $F > 4\sigma(F)$, S = 1.038). The final atomic coordinates, and crystallographic data for structure (4) have been deposited to the Cambridge Crystallographic Data Centre, 12 Union Road, CB2 1EZ, UK (fax: +44-1223-336033; e-mail: deposit@ccdc.cam.ac.uk) and are available on request quoting the deposition numbers CCDC 1934743).

### 2.3. Theoretical calculations

*Crystal Explorer* 17.5 was utilized to generate fingerprint plots and Hirshfeld surface map of the title compound (4) [20]. The conformations of the title compound were optimized using m06-2x/cc-pvdz method [21]. Character of the stationary point on potential energy surface was checked by calculations of Hessian at the same level of theory. All stationary points possess zero imaginary frequencies. All the quantum chemical calculations were carried out using Gaussian 09 [22]. The Quantum Theory Atoms in Molecule (QTAIM) analysis was carried out using wave function obtained at the same level of theory with the use of AIMAll program [23].

The pharmacophore model generation and docking were performed using Ligandscout 4.3 program [24].

### 2.4. Biological activity test

The experiment protocol is the following [15]. HepAD38 cells were passaged in a DMEM medium containing 10% fetal calf serum, penicillin/streptomycin and essential amino acids. The culture medium was taken once every 2 days, clarified by centrifugation (200 g, 15 min) and stored at 4 °C for no longer than 7 days. Next, dry PEG 8000 was added to the culture media to a final concentration of 7.5% and incubated at 4 °C on a rotary platform overnight. The viral precipitate was separated by centrifugation (2000 g, 30 min) and the precipitate was suspended in 1/100 of the initial volume in OPTI-MEM medium. Thus obtained viral preparation was aliquoted and stored at −80 °C.

Infection was carried out as follows: The HepG2-NTCP cell suspension was distributed to 96-well plates at 2000 cells per well. After the cells were attached (on the same or the next day), the initial solution was removed by aspiration, and 50 μL of a solution of test compound dissolved in OPTI-MEM medium (with a final DMSO concentration of 2%) was added to each well or OPTI-MEM with 2% DMSO (in the wells of the positive and negative controls of the infection) and 50 μL of the HBV preparation diluted in OPTI-MEM with 2% DMSO (except negative infection control). After incubation for 24 h in a humidified atmosphere containing 5% $CO_2$, the HBV medium was removed by aspiration, and 200 μL of DMEM culture medium containing the corresponding test compound in 10 mkM concentration was added to the cultures. The cells were additionally incubated for 6 days at 37 °C in a humidified atmosphere containing 5% carbon dioxide. Next, cell supernatants (50 μL) were analyzed for viral antigen content using a commercial HBeAg ELISA 4.0 kit (Creative Diagnostics, catalog number DEIA003) according to the kit manufacturer's protocol and the optical density of each analyzed well

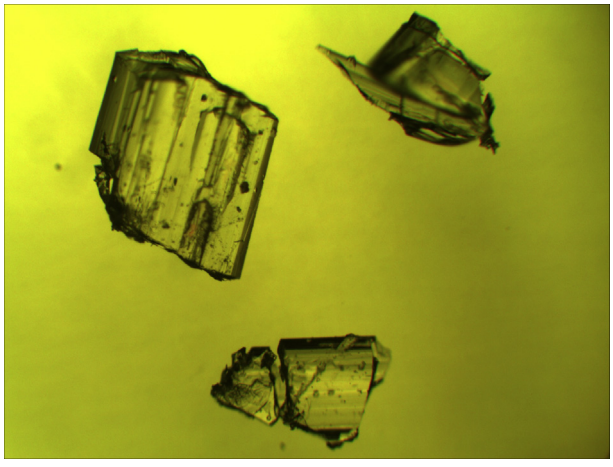

**Fig. 3.** Crystals of the title compound (4).

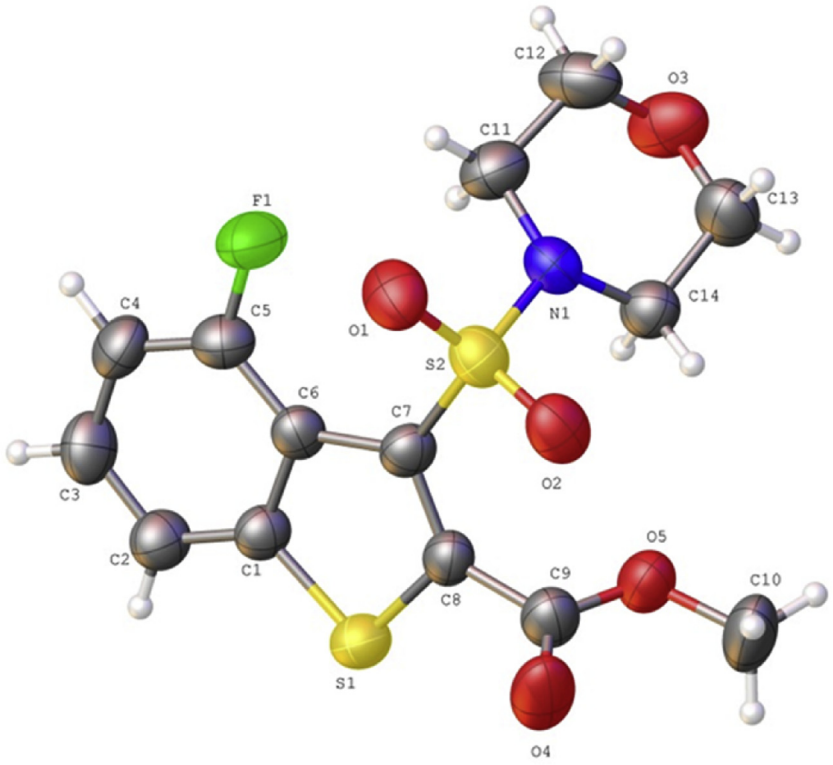


**Fig. 4.** Molecular structure of the title compound (4). Thermal ellipsoids are shown at 50% probability level.

**Table 1**
Geometric characteristics of the hydrogen bonds in the crystal of compound (4).

| Hydrogen bond | Symmetry operations | H···A, Å | D—H···A, ° |
|---|---|---|---|
| C2-H2…O1 | x, 0.5-y,-0.5+z | 2.60 | 133 |
| C4-H4…O4 | -1+x, y, z | 2.54 | 169 |
| C12-H12B…F1 | 2-x, 1-y, 1-z | 2.60 | 120 |

was measured at a wavelength of 450 nm using a plate densitometer [35].

## 3. Results and discussion

The initial methyl 3-amino-4-fluorobenzo[b]thiophene-2-carboxylate (1) was obtained according to the method described earlier [25]. Then 3-amino-4-fluorobenzo[b]thiophene-2-carboxylate (1) was diazotized and treated with $SO_2$ to give methyl 3-(chlorosulfonyl)-4-fluorobenzo[b] thiophene-2-carboxylate (2) which was employed in the next reaction stage without additional purification. Further product (2) was converted to the title compound (4) by mechanical stirring with morpholine (3) in DMF medium (see Scheme 1) .

The obtained compound (4) was studied using UV-, IR-, $^{1}$H NMR, $^{13}$C

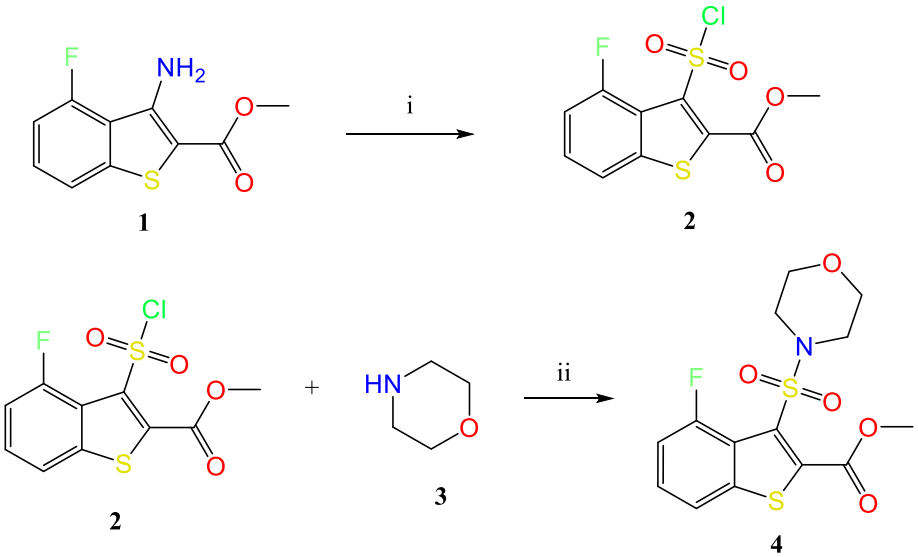


**Scheme 1.** Synthesis of the methyl 4-fluoro-3 (morpholinosulfonyl)benzo[b]thiophene-2-carboxylate (4): (i) – $NaNO_2$, HCl, HOAc, $SO_2$, CuCl, -10 °C; (ii) – DMF, 1h at 60 °C.

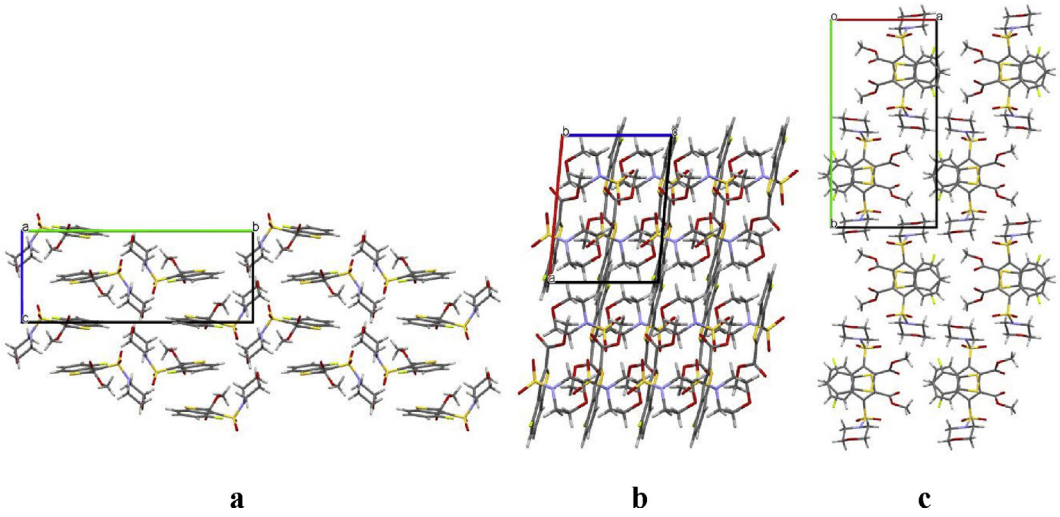


**Fig. 5.** Packing of molecules (4) in the crystal phase. a- Projection along *a* crystallographic axis, b- Projection along *b* crystallographic axis, c- Projection along *c* crystallographic axis.

NMR and $^{19}$F NMR spectra (Supporting Information, Figs. S1-S5) as well as LC/MS data for structural determination (Fig. S6). Finally, the structure of the title compound was confirmed by X-ray analysis (Fig. 4).

According to the X-ray diffraction data all atoms of the benzothiophene fragment lie in the plane within 0.02 Å. The morpholine ring adopts a chair conformation (the puckering parameters [26] are S = 1.16, Θ = 3.3°, Ψ = 19.8°). Deviations of the N1 and O3 atoms from the mean-square plane of the remaining atoms of this ring are -0.61 Á and 0.66 Á respectively. The morpholine substituent is almost orthogonal to the C7-C8 endocyclic double bond (the C8-C7-S2-N1 torsion angle is 101.8(3)°) and it is turned with respect to the C7-S2 bond (the C7-S2-N1-C11 torsion angle is 75.4(3)°). Such position of this group leads to the appearance of the H11A…F1 2.50 Å (van der Waals radii sum [27] 2.62 Å) shortened intramolecular contact which cannot be considered as hydrogen bond owing to very small value of the C-H…F angle (110°).

The presence of vicinal substituents at the C7–C8 endocyclic double bond causes disturbing of conjugation between π-systems of bicyclic fragment and carboxylic fragment of the ester group. The ester substituent is turned significantly to the bicycle (the C7-C8-C9-O5 torsion angle is -76.5(5)°) and its methyl group is located in *ap*-conformation in relation to the C8-C9 bond (the C8-C9-O5-C10 torsion angle is 179.7(4)°). The C9…O2 shortened intramolecular contact (the distance is 2.65 Å as compared to the van der Waals radii sum 3.00 Å) is observed between vicinal substituents.

In the crystal phase, molecules 4 form columns along the [0 0 1] crystallographic direction. Molecules within a column are bound by very weak C2-H2…O1 intermolecular hydrogen bond and interaction between bicyclic fragments (the angle between bicyclic planes is 15.1° and the distance between centroids is 3.841 Á) (Table 1). The molecules within the columns are arranged in “head-to-tail” type (Fig. 5). The molecules of neighbouring columns are bound by the C4-H4…O4, C12-H12B…F1 and C10-H10B…C13 weak intermolecular hydrogen bonds (Table 1).

The crystal packing peculiarities are caused by the molecule ability to form certain types of intermolecular interactions. On the other hand, the biological activity depends on the formation of intermolecular interactions between the target molecule and the corresponding receptor. Therefore the study of intermolecular interactions is a very important task.

One of the newest methods of the intermolecular interactions analysis in the crystal phase is the study of Hirshfeld surfaces and 2D fingerprint plots generated by the *CrystalExplorer* program [20]. The Hirshfeld surfaces and their associated 2D fingerprint plots for the title compound (4) were calculated taking the single-crystal X-ray data as input. The Hirshfeld surface emerged from an attempt to define the space occupied

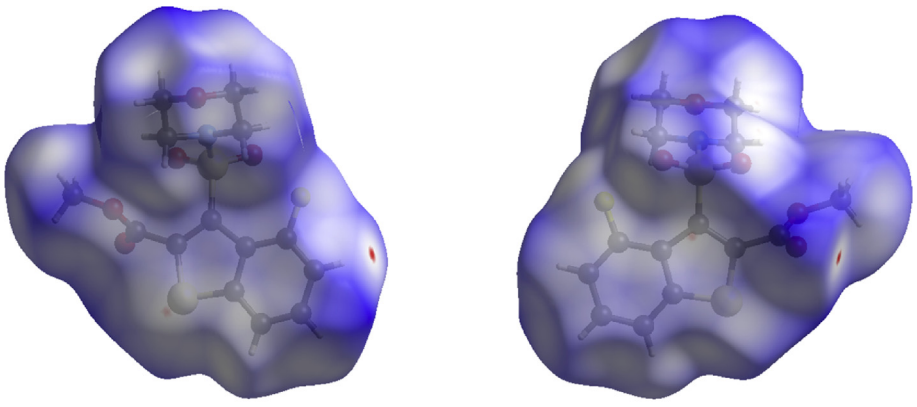


**Fig. 6.** The Hirshfeld surface of the titled compound (4) mapped with $d_{norm}$(projection a and b).

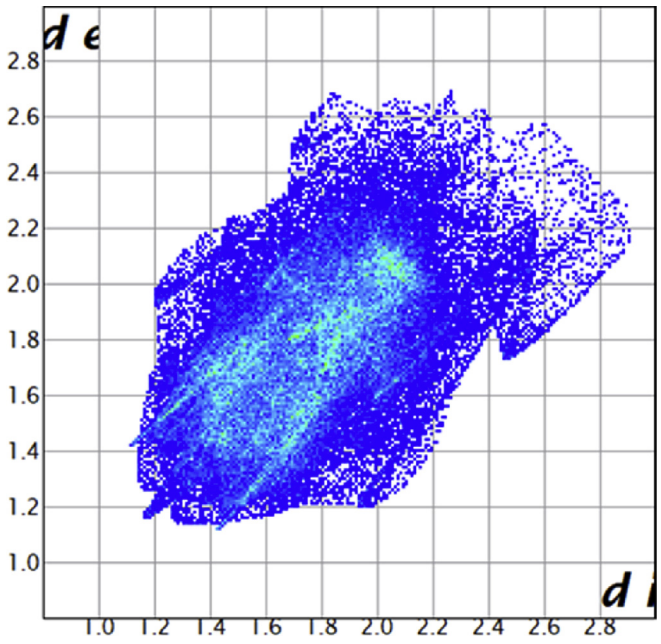

**Fig. 7.** Fingerprint plot of the title compound.

by a molecule in a crystal for the purpose of partitioning the crystal electron density into molecular fragments [28]. It provided a 3D picture of the close contacts in the crystal, and these contacts can be summarized in a fingerprint plot [29]. The areas of the short contacts are shown by a red color on the Hirshfeld surfaces, while the long distances can be detected as blue areas (Fig. 6). The intermolecular interactions outward the H···H/O···H/F···H/C···C/S···O/S···H/C···S/C···H contacts, as well as the overall fingerprint region of the title molecule, are displayed in Fig. 7. With this analysis, the division of contributions is possible for different interactions including H···H, O···H, C···S, and C···H, which commonly overlap in the full fingerprint plots. Fig. 8 shows the $d_{norm}$ surface of compound (4), the contribution of the O…H/H…O contacts, corresponding to the C-H…O interactions, is represented by a pair of sharp spikes (29.0%). The absence of long sharp spikes indicates the absence of strong hydrogen bonds in the crystal of the title compound (4) (Fig. 8).

Using computational methods for studying the properties of potentially biological active molecules allows us to predict its behavior in the real environment. To clarify the effects of ligand incorporation into protein we have performed the calculation of title molecule geometry. The M06-2x DFT functional with cc-pVDZ basis set has been used. The torsion angles shown in Table 2 are the most important parameters that are closely related with the molecular conformation. We have described two conformations that are important in the description of the interaction between ligand and protein. They were generated by the rotation around the C7-S2 and S2–N1 single bonds (Fig. 9). The energy differences between the more stable conformers were rather small and amounted to

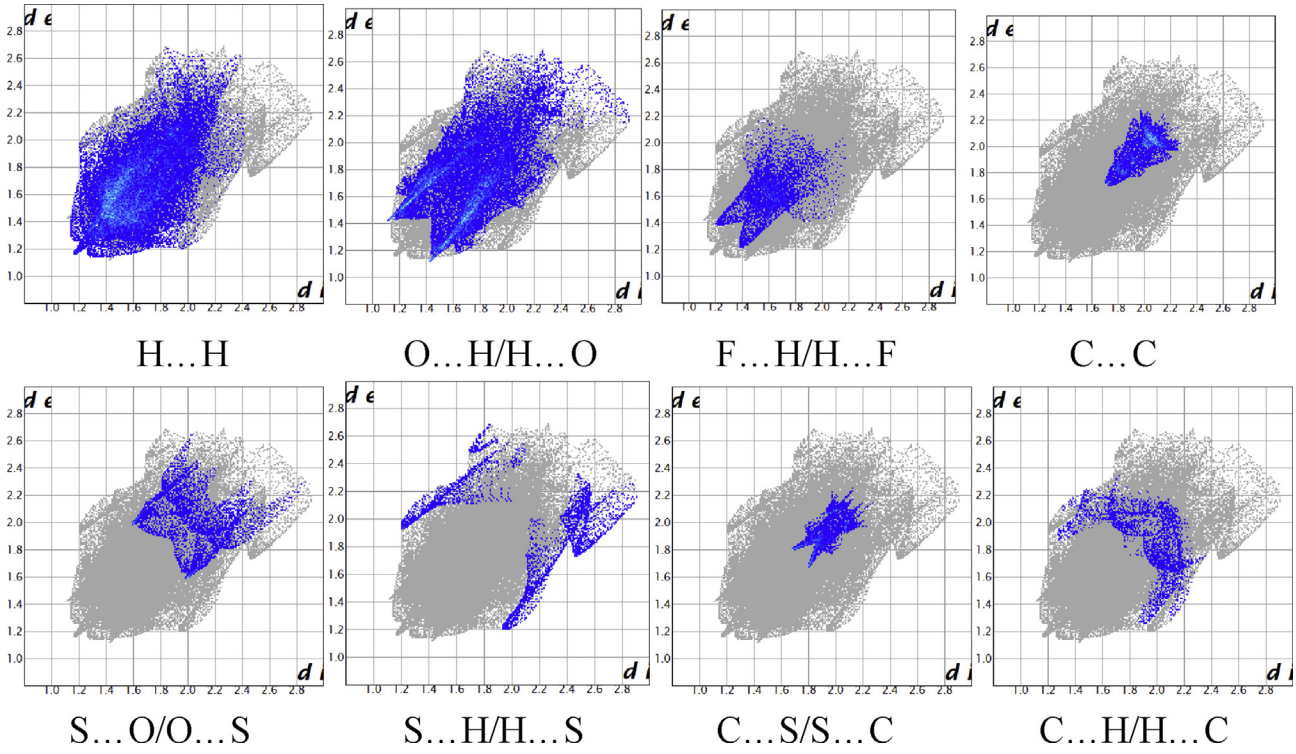


**Fig. 8.** Two-dimensional fingerprint plots with a $d_{norm}$ view of the H…H (36.1%), O…H/H…O (29.9%), F…H/H…F (6.4%), C…C (6.1%), S…O/O…S (5.1%), S…H/H…S (4.0%), C…S/S…C (3.6%) and C…H/H…C (3.5%) contacts in the title compound.

**Table 2**
Selected torsion angles of the title molecule according to the quantum chemical calculations as compared to the experimental and docking data.

| Torsion angle, deg | Conf1 | Conf2 | X-ray | Docking |
|---|---|---|---|---|
| N1–S2–C7–C8 | 103.7 | -92.9 | 101.8 | -98.1 |
| C7–C8–C9–O5 | 70.1 | 46.3 | 76.5 | 55.0 |
| C7–S2–N1–C11 | 71.7 | -88.6 | 75.4 | -56.0 |
| C8–C9–O5–C10 | 171.5 | 173 | 179.7 | 83.0 |

-0.94 kcal/mol. The values of selected torsion angles are collected in Table 2. The atom numerations are corresponded to Fig. 4.

As one can see, the calculated torsion angles of less stable conformer 1 were rather close to those obtained in the crystal phase (Table 2) while the values of torsion angles in more stable conformer 2 demonstrated significant differences between the experimental and calculated values. Taking into account very small difference in energy between two conformers calculated in vacuum approach we can presume that the

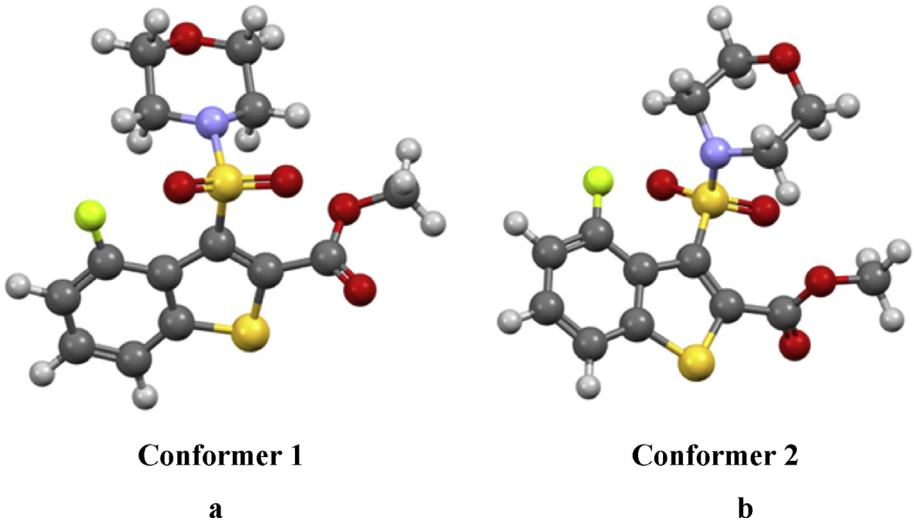


**Fig. 9.** Two conformations (a and b) of the title compound calculated by m06-2x/cc-pvdz method.

presence of conformer 1 in the crystal phase is caused by the packing effects. The difference in molecular conformations means the presence of different intramolecular contacts stabilizing the certain molecular form. The modern method of intramolecular interactions studying is the analysis of electron density distribution using the Bader's theory "Atoms in Molecules" (AIM) [30]. This theory allows transition from qualitative to quantitative analysis of electron density ρ(r). Within this theory, each the electron density extremum in three-dimensional space is described by a corresponding critical point. For example, each atom is described by a (3, -3) critical point, and each chemical bond or intermolecular interactions are described by a (3, -1) critical point. Moreover, this method allowed to estimate the energy of intramolecular interactions using Espinosa's correlation equation: $E_{cont} = 0.5\ V(r)$, where V(r) is a value of local potential energy in bond critical point (BCP) of intermolecular contact [31]. The contact energies obtained from the Espinosa's correlation equation for all intramolecular interactions found in two conformers are shown in Fig. 10.

The results showed that four bond critical points (BCP) in Conformer 1 and seven BCPs in Conformer 2 were found. The contact energies vary in the range from 2.57 to 4.11 kcal/mol in Conformer 1 and from 1.73 to 4.19 kcal/mol in Conformer 2 (Fig. 10). It can be assumed that Conformer 2 is more stable due to a greater number of intramolecular interactions, which correlates well with relative stability (Conformer 2 on 0.94 kcal/mol more stable than Conformer 1).

The next stage of our study was molecular modeling of the potential interaction of the target molecule with receptors before conducting experimental tests on the biological activity in order to find out which of the conformations is realized when the title molecule interacts with receptors.

The title molecule (4) has been tested as a system which interacts with the capsid of HBV (Hepatitis-B virus). The main approach to anti-HBV agents' development is associated with the search of potent inhibitors of HBV replication [32, 33, 34, 35]. Such ligands demonstrate effective interactions with corresponding HBV capsid and newly synthesized core protein. After ligand-protein interaction the core protein cannot assemble properly. Among the most important proteins there are 5E0I, 5GMZ, 5WRE and 5T2P which can be obtained from protein Data Bank [36].

In the present study we performed the virtual screening and docking of the title molecule with above mentioned proteins using LigandScout 4.3 program [24]. For the above mentioned structures of proteins there are six chains (designated as A, B, C, D, E, and F). The residual mean square deviation (RMSD) between docking-generated poses for reference molecule and ones obtained from X-ray crystal structure study were calculated. The minimal values of RMSD, calculated for all the above

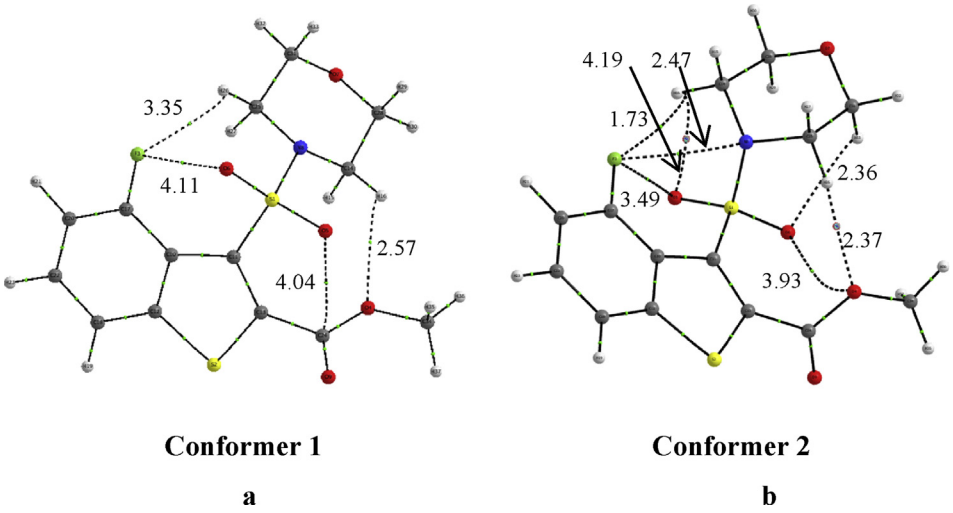


**Fig. 10.** Molecular graphs of title molecule conformers (a and b) obtained from the analysis of electron density distribution using the Bader's theory "Atoms in Molecules" (AIM). All values of intramolecular contact energies are given in kcal/mol.

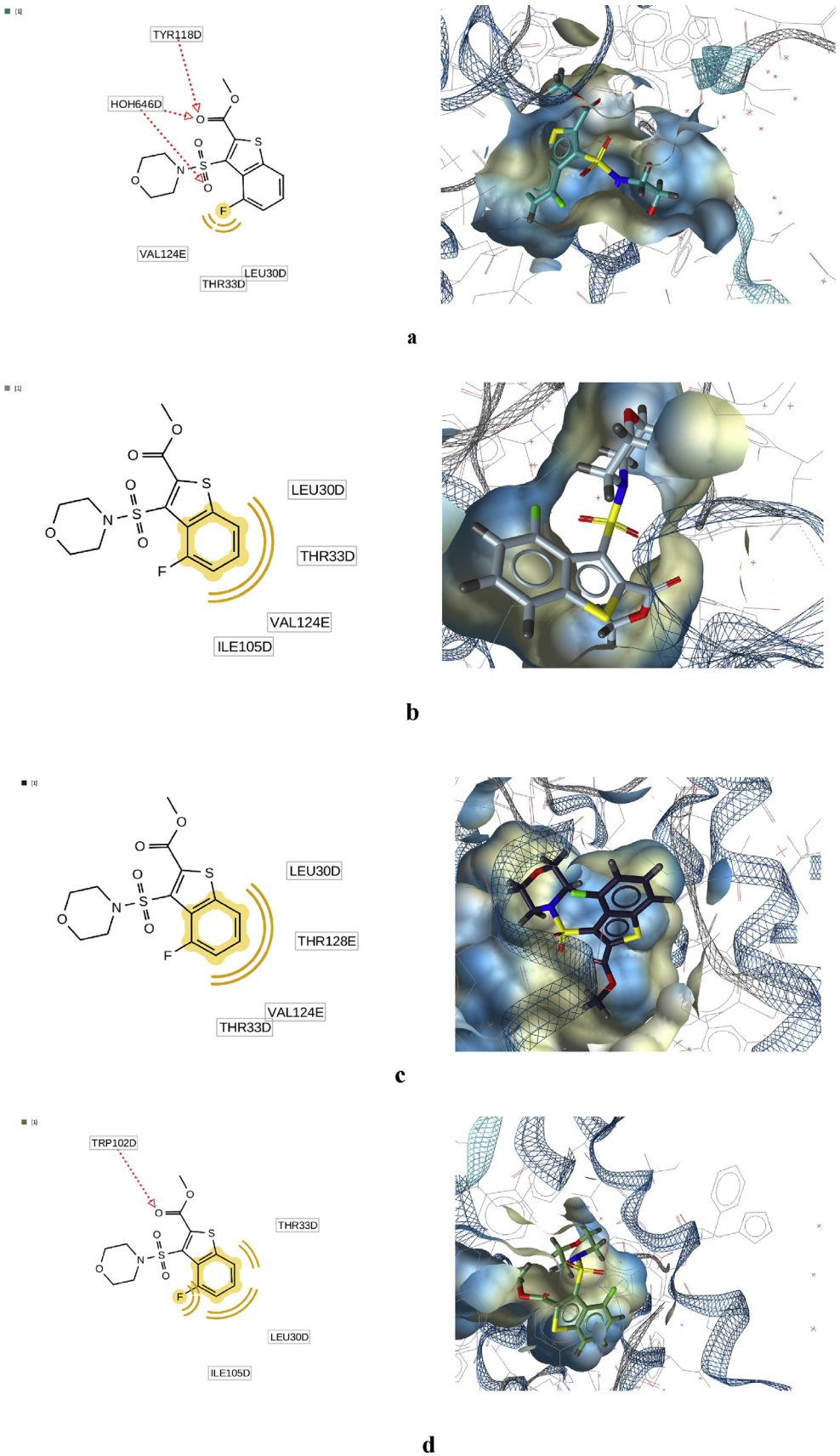


**Fig. 11.** Generated docking pose for complexes "title molecule — protein" (a-interaction with 5E0I protein, b-interaction with 5GMZ protein, c-interaction with 5WRE protein, and d-interaction with 5T2P protein).

**Table 3**
Selected parameters of title molecule docking with proteins.

| Protein | Binding Affinity Score | Est. Binding Energy (kcal/mol) |
|---|---|---|
| 5E0I | -28.39 | -15.96 |
| 5GMZ | -19.15 | -14.80 |
| 5WRE | -16.18 | -14.78 |
| 5T2P | -32.37 | -16.50 |

**Table 4**
HBV inhibition *in vitro* measuring with the HepAD38 line, carrying the stably integrated HBV genome under the tetracycline-regulated promoter control.

| Primary data, OD | | Mean signal, 3 wells | SD | % INH/AC ($OD_{Pos}$-$ID_{Test}$)/($OD_{Pos}$-$OD_{Neg}$) *100% | p-value |
|---|---|---|---|---|---|
| Negative control, DMSO 2% | | 0.12 | 0.17 | | |
| Title compound, | 32 | 7.76 | 0.26 | 84.98 | 0.0119 |
| concentration, | 10 | 31.90 | 0.46 | 37.54 | 0.0694 |
| мкМ | 3.2 | 39.50 | 0.34 | 22.60 | 0.1731 |
| Positive control, DMSO 2%, HBV | | 47.00 | 0.40 | | |

mentioned proteins are correspond to D-chain, where RMSD <1 Å. The active site as well as pharmacophore structure was found using corresponding LigandScout option. The resulting docking poses are presented in Fig. 11.

Selected docking parameters are collected in Table 3. For the detailed description of estimated parameters and pharmacophore selection see LigandScout 4.3 manual. One can see that the title molecule has significant interaction with corresponding proteins.

The "receptor-ligand" complexes (proteins are 5E0I, 5GMZ, 5WRE and 5T2P) can be seen in Fig. 11. Here the plain 2D representation of correspondence of ligand to generated parmacophore and special 3D structure of complexes is demonstrated. For the 2D picture the hydrogen bonds are designated with the red dotted line, while the hydrophobic interaction is designated with the yellow one.

The obtained geometrical structure of the ligand in all the "ligand-protein" complexes was qualitatively close to more stable in vacuum conformer 2 (see Fig. 9 and Table 2). For instance for the complex of title molecule with 5E0I protein we obtained the following values (Table 3). Comparison of the corresponding data with conformer 2 from the *ab initio* calculations shows clearly the good agreement.

The docking of the title molecule with corresponding proteins demonstrated effective interaction. So compound (4) can be utilized as a potential inhibitor of HBV replications. It may ensure as a basis for further studies of the title molecule biological activity.

It should be noted that according to the calculations of calculations of the three-dimensional structure of "receptor-ligand" complex (Fig. 11), the morpholine part of the studied molecule does not participate in any interactions with the binding site. However, it is known that, in practice, molecules containing a morpholine fragment often exhibit higher biological activity than their analogues with other substituents [14].

We performed the study of the title molecule biological activity according to the experimental in vitro hepatitis B virus infection model with the usage of human hepatoma line HepG2 [34,35]. This model was designed in two manners in order to determine the precise stages of HBV infection development that is affected by the tested compound. Identification of the "viral entry" inhibitors could be visualized via the effect comparing for HBV infecting of the cultivated HepG2/NTCP cells before and after the tested compound adding.

**Table 5**
HBV inhibition *in vitro* measuring with the HepG2 line stably transfected with the NTCP gene.

| Primary data, OD | | Mean signal, 3 weals | SD | % INH/AC ($OD_{Pos}$-$ID_{Test}$)/($OD_{Pos}$-$OD_{Neg}$) *100% | p-value |
|---|---|---|---|---|---|
| Negative control, DMSO 2% | | 0.10 | 0.21 | | |
| Title compound, | 32 | 0.36 | 0.26 | 99.44 | 0.0017 |
| concentration, | 10 | 9.91 | 0.31 | 79.08 | 0.0134 |
| мкМ | 3.2 | 24.50 | 0.76 | 47.97 | 0.0513 |
| Positive control, DMSO 2%, HBV | | 47.00 | 0.34 | | |

For the further confirmation of the action stage for the title compound, a model of either a) the HepAD38 human hepatoma cell line, carrying the stably integrated HBV virus genome under the tetracycline-regulated promoter control [37] or b) the HepG2 line stably transfected with the NTCP gene [15] maintaining a full virus replication cycle. Contrary in the first model design the stage of penetration of the virus into the cell is absent. Using this model, inhibitors of the infection development acting only at the stages following the penetration of the nucleocapsid into the cell could be detected and measured, while inhibitors of the interaction of the viral particle with core NTCP could be identified in the second model only.

The primary results obtained for the title compound in the both models are given in Tables 4 and 5 consequently.

As we see from the tables, the title compound (4) reliably demonstrated in vitro hepatitis B virus infection inhibition in 10 μM concentration in the second model (with the usage of human hepatoma line HepG2 stably transfected with the NTCP gene) and significant but not reliable inhibition in the HepAD38 human hepatoma cell line, carrying the stably integrated HBV virus genome under the tetracycline-regulated promoter control model (79 % and 37 % consequently). Taking into account low cytotoxicity of the tested compound it could be identified as a rather promising "viral entry" inhibitor.

Currently no "small molecule" NTCP-associated viral inhibitor is observed on the market. The only FDA-approved HBV-entry receptor inhibitor is Myrcludex B, a synthetic peptide with picomolar activity [38] but with all problems associated with its nature such as short plasma half-life due to unstable in front of digestive enzyme system amide bonds in proteins and negligible oral bioavailability in view of high polarity and molecular weight of peptides severely limiting intestinal permeability [39]. As oral delivery seems highly attractive for long-playing therapy synthetic small molecules sound much better in this concern. The tested for viral entry inhibition zafirlukast ($IC_{50}$ 6.5 μM), TRIAC ($IC_{50}$ 6.9 μM), and sulfasalazine ($IC_{50}$ 9.6 μM) demonstrated comparable to our substance activity [38]. As viral entry inhibition is a promising approach to prevent development of resistant viral forms elaboration a new NTCP-associated HBV inhibitor development seems to be an inspirational task.

## 4. Conclusions

The new biologically active compound of 4-fluoro-3-(morpholinosulfonyl)benzo[b]thiophene-2-carboxylate has been studied using both theoretical and experimental methods. The title compound was characterized by spectral methods and the molecular and crystal structure has been confirmed by X-ray diffraction study. At the first stage, it was shown the existence of two the most stable conformers which realized in vacuum, X-ray and docking study. Being very important to provide the interaction with receptors intermolecular interactions were studied thoroughly. Some approaches to quantum chemical modeling of possible interaction of the title molecule with receptors have been used. Finally, the experimental study of biological activity has shown that a promising drug for hepatitis B treatment has been developed.

## Declarations

### *Author contribution statement*

Alexandre V. Ivachtchenko, Oleg D. Mitkin: Conceived and designed the experiments; Analyzed and interpreted the data; Contributed reagents, materials, analysis tools or data; Wrote the paper.

Dmitry V. Kravchenko, Sergiy M. Kovalenko: Conceived and designed the experiments; Analyzed and interpreted the data.

Svitlana V. Shishkina, Irina S. Konovalova: Performed the experiments; Analyzed and interpreted the data.

Natalya D. Bunyatyan, Irina G. Dmitrieva: Analyzed and interpreted the data; Contributed reagents, materials, analysis tools or data; Wrote the paper.

Vladimir V. Ivanov, Thierry Langer: Performed the experiments; Analyzed and interpreted the data; Contributed reagents, materials, analysis tools or data.

*Funding statement*

This work was supported by Ministry of Science and Higher Education of the Russian Federation in frames of Agreement on reimbursement of costs associated with Development of a platform for biologically active compound libraries design for actual biotargets, including the platform testing on the example of invention and 500 preparation of candidate libraries for HBV treatment designed as inhibitors of viral penetration and assembly of viral core particles (RFMEFI57917X0154).

*Competing interest statement*

The authors declare no conflict of interest.

*Additional information*

Supplementary content related to this article has been published online at https://doi.org/10.1016/j.heliyon.2019.e02738.

## References

[1] M. Pieroni, E. Azzali, N. Basilico, S. Parapini, M. Zolkiewski, C. Beato, G. Annunziato, A. Bruno, F. Vacondio, G. Costantino, Accepting the invitation to open innovation in malaria drug discovery: synthesis, biological evaluation, and investigation on the structure–activity relationships of benzo[b]thiophene-2-carboxamides as antimalarial agents, J. Med. Chem. 60 (2017) 1959–1970.

[2] C. Mitsui, T. Okamoto, M. Yamagishi, J. Tsurumi, K. Yoshimoto, K. Nakahara, J. Soeda, Y. Hirose, H. Sato, A. Yamano, T. Uemura, J. Takeya, High-performance solution-processable N-shaped organic semiconducting materials with stabilized crystal phase, Adv. Mater. 26 (2014) 4546–4551.

[3] I. Osaka, S. Shinamura, T. Abe, K. Takimiya, Naphthodithiophenes as building units for small molecules to polymers; a case study for in-depth understanding of structure–property relationships in organic semiconductors, J. Mater. Chem. C 1 (2013) 1297–1304.

[4] L. Berrade, B. Aisa, M.J. Ramirez, S. Galiano, S. Guccione, L.R. Moltzau, F.O. Levy, F. Nicoletti, G. Battaglia, G. Molinaro, I. Aldana, A. Monge, S. Perez-Silanes, Novel benzo[b]thiophene derivatives as new potential antidepressants with rapid onset of action, J. Med. Chem. 54 (2011) 3086–3090.

[5] Z. Qin, I. Kastrati, R.E.P. Chandrasena, H. Liu, P. Yao, P.A. Petukhov, J.L. Bolton, G.R.J. Thatcher, Benzothiophene selective estrogen receptor modulators with modulated oxidative activity and receptor affinity, J. Med. Chem. 50 (2007) 2682–2692.

[6] B.L. Flynn, E.M. Hamel, K. Jung, One-pot synthesis of benzo[b]furan and indole inhibitors of tubulin polymerization, J. Med. Chem. 45 (2002) 2670–2673.

[7] C.-N. Hsiao, T. Kolasa, Synthesis of chiral zileuton, a potent and selective inhibitor of 5-lipoxygenase, Tetrahedron Lett. 33 (1992) 2629–2632.

[8] S. Purser, P.R. Moore, S. Swallow, V. Gouverneur, Fluorine in medicinal chemistry, Chem. Soc. Rev. 37 (2008) 320–330.

[9] J.E. Lesch, The First Miracle Drugs: How the Sulfa Drugs Transformed Medicine, Oxford University Press, Oxford, New York, 2007, p. 364.

[10] N. Blok, C.Wu, P. Woodard, K. Keller, T. Kogan, Formulation of Sulfonamides for Treatment of Endothelin-Mediated Disorders, International Patent Application Publication No. US 6248767 B1, 19 June 2001.

[11] M. F. Chan, C. Wu, B. G. Raju,T. Kogan, A. Kois, E. Joel, V. Rosario, S. Castillo, V. Yalamorri, V. N. Balaji, Thienyl-, Furyl- and Pyrrolyl-Sulfonamides and Derivatives Thereof that Modulate the Activity of Endothelin, International Patent Application Publication No. US 5962490 A, 5 October 1999.

[12] C. de Wu, N. Blok, T. Kogan, K. Keller, P. Woodard, Sulfonamides for Treatment of Endothelin-Mediated Disorders, International Patent Application Publication No. WO 9849162 A1, 11 May 1998.

[13] M. F. Chan, B. G. Raju, A. Kois, E. J. Verner, C. Wu, R. S. Castillo, V. Yalamoori, V. N. Balaji, Thienyl-, Furyl- and Pyrrolyl Sulfonamides and Derivatives Thereof that Modulate the Activity of Endothelin, International Patent Application Publication No. US 5594021 A, 14 January 1997.

[14] A. Kourounakis, D. Xanthopoulos, A. Tzara, Morpholine as a privileged structure: a review on the medicinal chemistry and pharmacological activity of morpholine containing bioactive molecules, Med. Res. Rev. (2019, Sep. 12).

[15] Hepatitis B Virus: Methods and Protocols, in: H. Guo, A. Cuconati (Eds.), Methods in Molecular Biology, 1540, Springer Science+Business Media LLC, 2017.

[16] A. Ivashchenko, O. Mitkin, D. Kravchenko, I. Kuznetsova, S. Kovalenko, N. Bunyatyan, Th. Langer, Synthesis, X-ray crystal structure, Hirshfeld surface analysis, and molecular docking study of novel hepatitis B (HBV) inhibitor: 8-Fluoro 5-(4-fluorobenzyl)-3-(2-methoxybenzyl)-3,5-dihydro-4Hpyrimido[5,4-b]indol-4-one, Crystals 9 (8) (2019) 379–393.

[17] A. V. Ivachtchenko, A. A. Ivachtchenko, N. Ph. Savchuk, B. Rogovoj, V. V. Bychko, Hepatitis B Virus (HBV) Inhibitor. International Patent Application Publication No. WO 2019017814 Jan 24, 2019.

[18] A. V. Ivachtchenko, A. A. Ivachtchenko, N. Ph. Savchuk, B. Rogovoj, V. V. Bychko, A. Khvat, Hepatitis B Virus (HBV) Penetration Inhibitor and Pharmaceutical Composition for Hepatitis Treatment, International Patent Application Publication No. RU 2662161 Jul 24, 2018.

[19] G.M. Sheldrick, SHELXT—integrated space-group and crystal-structure determination, Acta Crystallogr. A71 (2015) 3–8.

[20] M.J. Turner, J.J. McKinnon, S.K. Wolff, D.J. Grimwood, P.R. Spackman, D. Jayatilaka, M.A. Spackman, Crystal Explorer 17, The University of Western Australia, Perth, Australia, 2017.

[21] Y. Zhao, D. Truhlar, The M06 suite of density functionals for main group thermochemistry, thermochemical kinetics, noncovalent interactions, excited states, and transition elements: two new functionals and systematic testing of four M06 functionals and 12 other functionals, Theor. Chem. Acc. 120 (1) (2008) 215–241.

[22] M.J. Frisch, G.W. Trucks, H.B. Schlegel, G.E. Scuseria, M.A. Robb, J.R. Cheeseman, G. Scalmani, V. Barone, B. Mennucci, G.A. Petersson, et al., Gaussian-09; Revision A.02, Gaussian, Inc., Wallingford, CT, USA, 2009.

[23] T.A. Keith, T.K. Gristmill Software, K.S. Overland Park, AIMAll (Version 14.11.23), 2014.

[24] G. Wolber, T. Langer, LigandScout: 3-D pharmacophores derived from protein-bound ligands and their use as virtual screening filters, J. Chem. Inf. Model. 45 (2005) 160–169. Available online: http://www.inteligand.com/ligandscout/. (Accessed 24 July 2019).

[25] J.D. Tomer IV, G.M. Shutske, D. Friedrich, Synthesis of the novel thieno[4,3,2-ef][1,4]benzoxazepine ring system: 4,5-Dihydro-3-(4-pyridinyl)thieno[4,3,2-ef][1,4]benzox-azepine maleate, J. Heterocycl. Chem. 34 (6) (1997) 1769–1772.

[26] N.S. Zefirov, V.A. Palyulin, E.E. Dashevskaya, Stereochemical studies. XXXIV†. Quantitative description of ring puckering via torsional angles. The case of six-membered rings, J. Phys. Org. Chem. 3 (1990) 147–158.

[27] Yu.V. Zefirov, P.M. Zorky, New applications of van der Waals radii in chemistry, Russ. Chem. Rev. 64 (1995) 415–428.

[28] M.A. Spackman, P.G. Byrom, A novel definition of a molecule in a crystal, Chem. Phys. Lett. 267 (1997) 215–220.

[29] M.A. Spackman, D. Jayatilaka, Hirshfeld surface analysis, CrystEngComm 11 (2009) 19–32.

[30] R.F.W. Bader, Atoms in Molecules: A Quantum Theory Oxford, 1990.

[31] E. Espinosa, E. Molins, C. Lecomte, Hydrogen bond strengths revealed by topological analyses of experimentally observed electron densities, Chem. Phys. Lett. 285 (1998) 170–173.

[32] D. Endres, M. Miyahara, P. Moisant, A. Zlotnick, A reaction landscape identifies the intermediates critical for self-assembly of virus capsids and other polyhedral structures, Protein Sci. 14 (6) (2005) 1518–1525.

[33] S.J. Stray, A. Zlotnick, BAY 41-4109 has multiple effects on Hepatitis B virus capsid assembly, J. Mol. Recognit. 19 (6) (2006) 542–548.

[34] I.G. Choi, Y.G. Yu, Interaction and assembly of HBV structural proteins: novel target sites of anti-HBV agents, Infect. Disord. - Drug Targets 7 (3) (2007) 251–256.

[35] A. Firdayani, C. Arsianti, A. Yanuar, Molecular docking and dynamic simulation benzoylated emodin into HBV core protein, J. Young Pharm. 10 (2) (2018) s20–s24.

[36] H.M. Berman, J. Westbrook, Z. Feng, G. Gilliland, T.N. Bhat, H. Weissig, I.N. Shindyalov, P.E. Bourne, The protein Data Bank, Nucleic Acids Res. 28 (2000) 235–242. Available online: http://www.rcsb.org/. (Accessed 24 July 2019).

[37] S.K. Ladner, M.J. Otto, C.S. Barker, K. Zaifert, G.H. Wang, J.T. Guo, C. Seeger, R.W. King, Inducible expression of human hepatitis B virus (HBV) in stably transfected hepatoblastoma cells: a novel system for screening potential inhibitors of HBV replication, Antimicrob. Agents Chemother. 41 (8) (1997 Aug) 1715–1720.

[38] J.M. Donkers, B. Zehnder, G.J.P. van Westen, M.J. Kwakkenbos, A.P. Jzerman, R.P.J. Oude Elferink, U. Beuers, S. Urban, FJ van de Graaf, Reduced hepatitis B and D viral entry using clinically applied drugs as novel inhibitors of the bile acid transporter NTCP, Sci. Rep. 7 (1) (2017, Nov 10) 15307.

[39] J.L. Lau, M.K. Dunn, Therapeutic peptides: historical perspectives, current development trends, and future directions, Bioorg. Med. Chem. 26 (10) (June 2018) 2700–2707.